*Joint International Topical Meeting on Mathematics & Computation and Supercomputing in Nuclear Applications (M&C + SNA 2007)*
Monterey, California, April 15-19, 2007, on CD-ROM, American Nuclear Society, LaGrange Park, IL (2007)

# A COMPUTATIONAL DOSIMETRIC COMPARISON BETWEEN MCNPX AND ATTILA OF THE MAMMOSITE RADIATION THERAPY SYSTEM

**J.J. Bergman and T.S. Palmer**
Oregon State University
Department of Nuclear Engineering and Radiation Health Physics
116 Radiation Center, Corvallis, OR 97331
bergman@ne.orst.edu; palmerts@ne.orst.edu

## ABSTRACT

The need for more accurate radiation therapy treatment planning is driving improvements in radiation transport calculations. In particular, the inclusion of patient specific anatomy and tissue density heterogeneities will be very important, particularly for treatment modalities that involve strong material discontinuities. The study presented here compares the application of the deterministic code Attila and Monte Carlo code MCNPX to an absorbed dose calculation for an implanted MammoSite breast cancer radiation therapy system in conjunction with the Varian VariSource VS2000 iridium-192 high dose rate source. An initial simplified model was developed in each code consisting of the VS2000 centered in a 30 cm diameter sphere of water where total dose deposition over the volume was calculated. For this scenario, the codes compared to each other within 3% difference. Phantom models of the MammoSite and VS2000 sources in water were then used to compare physics modeling between Attila and MCNPX and showed agreement within 1-2%. A final model using patient computed tomography data in Attila provided absorbed dose gradients through anatomical structures, presenting an introduction to the unique brachytherapy treatment planning capabilities of Attila.

*Key Words*: Brachytherapy, Monte Carlo, deterministic, computed tomography, dosimetry

## 1. INTRODUCTION

Current brachytherapy treatment planning codes rely on algorithm-calculated source parameters, such as those described in the American Association of Physicists in Medicine (AAPM) Task Group 43 publications [1,2]. However, to allow for faster planning, details concerning patient anatomy and density heterogeneity are typically not considered. More recent Monte Carlo-based treatment planning systems allow explicit modeling of source and patient geometry and more detailed physics calculations accounting for tissue differences, but can require extensive computation times. Users of Monte Carlo calculations must also carefully consider the effects of variance reduction techniques on dose distributions [3]. An alternative approach that addresses both the issues of computational speed and physics modeling is the use of deterministic transport codes. Attila (Transpire, Inc., Gig Harbor, WA), is a deterministic transport code [4] that calculates global photon and electron distributions in complex, user-defined geometries.

This paper will present a comparison of three-dimensional dose distributions from Attila and the general purpose Monte Carlo transport code MCNPX 2.5.0 (Los Alamos National Laboratory, Los Alamos, NM) for a patient case-study of an implanted MammoSite (Cytyc, Marlboro, MA)

high dose rate (HDR) breast cancer treatment applicator. The modeled brachytherapy source used in this study was the iridium-192 VariSource VS2000 (Varian Oncology Systems, Palo Alto, CA).

Initially, results are presented of a simple water phantom dose calculation to verify that both Attila and MCNPX compare well with previously modeled VS2000 source data. A second modeling scenario includes five of the aforementioned iridium sources aligned in an ellipsoid MammoSite balloon catheter correlating to the positions of patient-specific geometry. Source intensities are based upon the necessary dwell times for the treatment dose. This model was employed to evaluate the potential change in absorbed dose at material interfaces such as between tissue (water) and bone, and again to verify the physics comparison between Attila and MCNPX. A more detailed model in Attila investigates dose variation through patient specific anatomy generated by computed tomographic (CT) images.

## 2. METHODS

### 2.1. Brachytherapy Source Specification and Initial Problem Description

An initial simplified model was created with both Attila and MCNPX consisting of a 30 cm diameter liquid water sphere with the VS2000 iridium-192 source located at the center. Source encapsulation geometry and material specification were based upon manufacturer information presented in the Nuclear Regulatory Commission Registry of Radioactive Sealed Sources [5]. The source consists of two iridium metal pellets ($\rho$=22.42 g/cm$^3$), 2.5 mm in length and 0.35 mm in diameter, inserted end-to-end into the distal portion of a nitinol alloy wire ($\rho$=6.5 g/cm$^3$, 55.6% nickel, 44.4% titanium by weight) with an outer diameter of 0.635 mm and wall thickness of 0.0035 inches. Fig. 1 shows the configuration of the source as modeled; note that the entire proximal length of the nitinol wire was not included in the model. The energy spectrum used in each code for the source was derived from the work presented by Glasgow and Dillman [6].

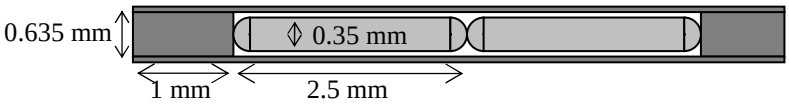


**Figure 1. Modeled VS2000 $^{192}$Ir source.**

Table I provides iridium-192 photon energies selected for the Attila and MCNPX simulations. The "Yield" column gives the intensity per decay of photons emitted, and can be represented by the number of photons per decay. The energies have been grouped by their associated specific gamma ray constant ($\Gamma$). As shown in Glasgow, the $\Gamma$ value listed for each energy is calculated using the mass attenuation coefficient, which is the probability of the photon of a particular energy being absorbed in any given material. By grouping the energies by $\Gamma$, the energies are more closely related to the energy absorption leading to dose. Selection of cut-off energies was determined by using the running sum fraction of the product of the energies and corresponding yields.

**Table I. Iridium-192 photon energies used for simulations**

| Decay Mode | Radiation Type | Energy (MeV) | Yield (frac/dis) | E*Y (MeV/dis) | Γ (R cm$^2$ mCi$^{-1}$ h$^{-1}$) | E*Y (running frac) |
|---|---|---|---|---|---|---|
| Beta | Gamma ray | 0.31650 | 8.28E-01 | 2.62E-01 | 1.48E+00 | 0.320 |
| Beta | Gamma ray | 0.46806 | 4.78E-01 | 2.24E-01 | 1.30E+00 | 0.593 |
| Beta | Gamma ray | 0.30845 | 2.97E-01 | 9.16E-02 | 5.15E-01 | 0.705 |
| Beta | Gamma ray | 0.29595 | 2.90E-01 | 8.58E-02 | 4.79E-01 | 0.810 |
| Beta | Gamma ray | 0.60440 | 8.18E-02 | 4.94E-02 | 2.86E-01 | 0.870 |
| Beta | Gamma ray | 0.61245 | 5.33E-02 | 3.26E-02 | 1.89E-01 | 0.910 |
| Beta | L-alpha 1 | 0.00944 | 1.55E-02 | 1.46E-04 | 1.61E-01 | 0.910 |
| Beta | Gamma ray | 0.58857 | 4.52E-02 | 2.66E-02 | 1.54E-01 | 0.943 |
| Beta | L-beta 1 | 0.01107 | 1.32E-02 | 1.46E-04 | 9.60E-02 | 0.943 |
| EC* | Gamma | 0.48456 | 3.16E-02 | 1.53E-02 | 8.87E-02 | 0.961 |
| EC | L-alpha 1 | 0.00891 | 6.38E-03 | 5.68E-05 | 7.40E-02 | 0.961 |
| Brem | Bremsstrahlung | 0.00500 | 1.40E-03 | 7.00E-06 | 5.47E-02 | 0.962 |
| EC | L-beta 1 | 0.01035 | 4.49E-03 | 4.65E-05 | 3.80E-02 | 0.962 |
| EC | Gamma | 0.20579 | 3.29E-02 | 6.77E-03 | 3.55E-02 | 0.970 |
| Brem | Bremsstrahlung | 0.00600 | 1.12E-03 | 6.72E-06 | 2.99E-02 | 0.970 |
| Beta | L-beta 2 | 0.01125 | 3.72E-03 | 4.19E-05 | 2.64E-02 | 0.970 |
| Beta | L-alpha 2 | 0.00936 | 1.73E-03 | 1.62E-05 | 1.83E-02 | 0.970 |
| Brem | Bremsstrahlung | 0.00700 | 9.20E-04 | 6.44E-06 | 1.77E-02 | 0.970 |
| Beta | K-alpha 1 | 0.06683 | 4.58E-02 | 3.06E-03 | 1.60E-02 | 0.974 |
| Beta | Gamma ray | 0.41646 | 6.62E-03 | 2.76E-03 | 1.59E-02 | 0.977 |
| EC | Gamma | 0.37448 | 7.29E-03 | 2.73E-03 | 1.57E-02 | 0.980 |
| Beta | Gamma ray | 0.88452 | 3.02E-03 | 2.67E-03 | 1.49E-02 | 0.984 |
| Beta | L-gamma 1 | 0.01294 | 2.60E-03 | 3.36E-05 | 1.35E-02 | 0.984 |
| EC | L-beta 2 | 0.01060 | 1.49E-03 | 1.58E-05 | 1.20E-02 | 0.984 |
| EC | Gamma | 0.48906 | 3.97E-03 | 1.94E-03 | 1.13E-02 | 0.986 |
| Brem | Bremsstrahlung | 0.00800 | 7.76E-04 | 6.21E-06 | 1.12E-02 | 0.986 |
| Beta | K-alpha 3 | 0.06451 | 2.88E-05 | 1.86E-06 | 9.98E-03 | 0.986 |
| Beta | K-alpha 2 | 0.06512 | 2.67E-02 | 1.74E-03 | 9.26E-03 | 0.988 |
| EC | L-alpha 2 | 0.00884 | 7.12E-04 | 6.29E-06 | 8.45E-03 | 0.988 |
| EC | K-alpha 1 | 0.06300 | 2.19E-02 | 1.38E-03 | 7.55E-03 | 0.990 |
| Brem | Bremsstrahlung | 0.00900 | 6.67E-04 | 6.00E-06 | 7.54E-03 | 0.990 |
| Brem | Bremsstrahlung | 0.01000 | 5.81E-04 | 5.81E-06 | 5.23E-03 | 0.990 |
| EC | L-gamma 1 | 0.01210 | 8.68E-04 | 1.05E-05 | 5.23E-03 | 0.990 |
| EC | Gamma | 0.20131 | 4.66E-03 | 9.38E-04 | 4.91E-03 | 0.991 |
| Beta | L-beta 3 | 0.01123 | 6.75E-04 | 7.58E-06 | 4.79E-03 | 0.991 |
| EC | K-alpha 2 | 0.06149 | 1.27E-02 | 7.81E-04 | 4.37E-03 | 0.992 |
| EC | L-beta 3 | 0.01051 | 5.23E-04 | 5.50E-06 | 4.29E-03 | 0.992 |
| EC | Gamma | 0.28326 | 2.61E-03 | 7.39E-04 | 4.10E-03 | 0.993 |
| Beta | L-beta 4 | 0.01085 | 5.16E-04 | 5.60E-06 | 3.93E-03 | 0.993 |
| Brem | Bremsstrahlung | 0.01100 | 5.13E-04 | 5.64E-06 | 3.78E-03 | 0.993 |
| Beta | K-beta 1 | 0.07575 | 1.03E-02 | 7.80E-04 | 3.75E-03 | 0.994 |

*Electron Capture (EC)

### 2.1.1. Air kerma source strength verification

A dose rate constant calculation ($\Lambda$, normalized with air kerma strength $S_k = K(d)d^2$ where $K(d)$ is the air kerma rate at a calibration distance $d$) was performed with MCNPX for the VS2000 to verify the source parameters used in the model. The calculation (1) is from the AAPM TG-43 formalism [1,2] where

$$\Lambda = \frac{D(r_o, \theta_o)}{S_k} \tag{1}$$

and $D(r_o,\Theta_o)$ is the dose rate at the reference distance $r_o$ = 1 cm from the source center line and $\Theta_o = \pi/2$. The value for $D(r_o,\Theta_o)$ was modeled as the absorbed dose to a 1 mm$^3$ cube of water, surrounded by water, with a source-center to cube-center distance of 1 cm. Air kerma strength $S_k$ was determined using a segmented surface tally of an 8 cm diameter circle inscribed on a sphere of air of radius 30 cm with the source located at the center. A value of 1.111±0.014 cGy h$^{-1}$ U$^{-1}$ was obtained from MCNPX and compared reasonably well with a previously reported dose rate constant by Angelopoulos et al. of 1.101±0.006 cGy h$^{-1}$ U$^{-1}$ where U = 1 unit of air kerma strength [7].

### 2.1.2. Brachytherapy device and dose region description

The MammoSite applicator consists of an expandable balloon catheter which is filled with iodine-containing contrast solution via an inflation channel to a shape of either a sphere or ellipsoid following a tumor lumpectomy, depending on device model [8]. A secondary inner closed-ended shaft allows for the placement of an iridium-192 HDR source without contacting the contrast solution or tissue. For this paper, five sources were modeled to simulate the single-source stepping required to provide a uniform dose distribution for an ellipsoid applicator. Fig. 2 shows the MammoSite ellipsoid and spherical balloon catheters. Fig. 3 shows a highlighted planning treatment volume (PTV) in a transverse sectional view that would receive at least 100% of the total prescription dose (34 gray) for the ellipsoid applicator; the PTV corresponds to a tissue distance of 1 cm from the balloon edge.

## 2.2. Phantom Modeling of MammoSite with MCNPX and Attila

A series of phantom models consisting of the ellipsoid MammoSite in water were used to verify particular aspects of the physics involved in dose deposition across anticipated interfaces and materials in MCNPX and Attila. Five VS2000 sources were modeled explicitly and positioned in a contrast-filled (90% water, 10% iodine, $\rho$ = 1.087 g/cm$^3$) ellipsoid balloon catheter, 4 cm diameter radius and 6 cm long, at the prescribed dwell positions derived from the patient data. Source strength was weighted based on prescribed dwell times for the treatment. The phantom was comprised of a 14 cm cube of water with the MammoSite long-axis centerline located 2.5 cm from the face center of one side of the water cube.

For three different models, the cube face nearest the balloon was extended outward 1 cm and changed to water, ICRU-defined bone ($\rho$ = 1.85 g/cm$^3$), and air. Additionally, a comparison between coupled photon and secondary electron transport, and photon only transport was

evaluated. A mesh tally of 0.5 cm voxels in MCNPX overlaid the geometry; the Attila model used nearly 2000 tetrahedral mesh cells with finer meshing in the regions of interest as shown in Fig. 4; Fig. 5 shows a cross-section of the analogous MCNPX model.

**Figure 2. MammoSite spherical and ellipsoid catheters.**

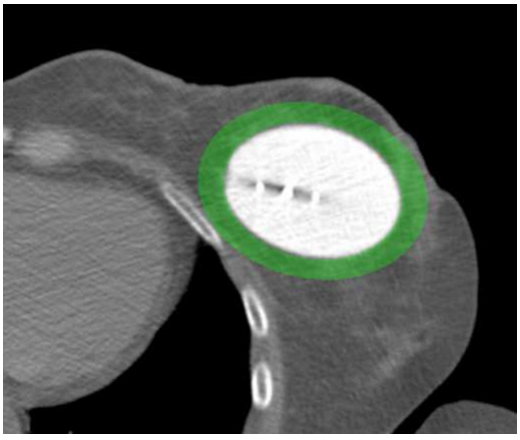

**Figure 3. PTV (green) for ellipsoid MammoSite applicator.**

### 2.2.1. Use of CT data for anatomical structure and dose-to-tissue modeling

Attila directly converts DICOM file formats (Digital Imaging and Communications in Medicine) into a geometry utilized by the code for radiation transport. A user-defined tetrahedral mesh is then superimposed over this geometry and is used by Attila to globally calculate energy

deposition. This method allows Attila to generate dose distributions in heterogeneous materials that comprise a specified geometry. For the model presented here, the five VS2000 sources were modeled incorporating the specific materials and dimensions defined by the manufacturer, and then converted to anisotropic point sources. Simulating the actual VS2000 sources in the phantom geometry would require prohibitively large spatial and angular resolution.

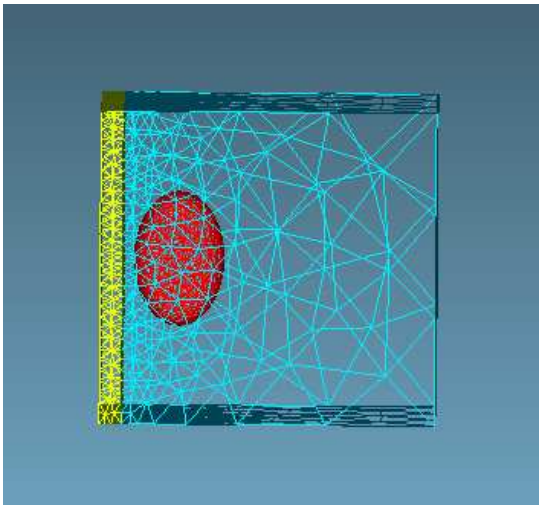

**Figure 4. Attila phantom geometry.**

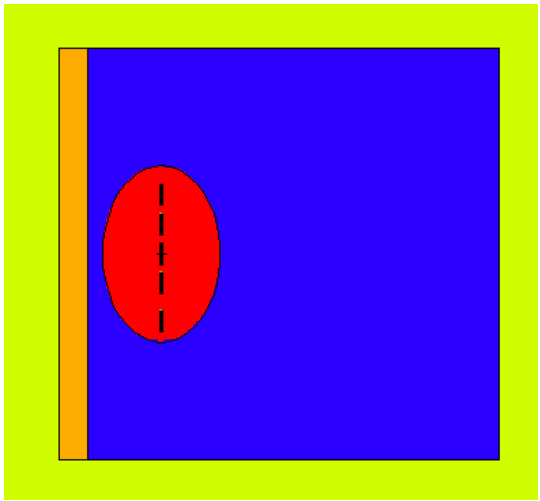

**Figure 5. MCNPX phantom geometry.**

# 3. RESULTS

## 3.1. Simplified Dose Model – 30 cm Diameter Sphere of Water

MCNPX, with 2e7 histories, calculated an absorbed dose to the entire water volume of 1.004e-5 MeV/g (0.0001 relative error) compared with Attila's calculated value of 1.031e-5 MeV/g – a difference of roughly 3% for the initial simplified model. The Attila calculation involved three steps. First, a resolved simulation of the VS2000, using an $S_{24}$ square Chebychev-Lobatto quadrature set, CEPXS cross-sections in 37 photon energy groups (see Table II), $P_3$ scattering and 42,537 tetrahedral cells was performed to generate an equivalent anisotropic point source. Fig. 6 shows the $\log_{10}$ of the flux distribution in the VS2000. This point source was then placed at the center of a sphere of water 15 cm in radius, and a ray trace was used to calculate the uncollided flux, minimizing ray effects. This uncollided flux was then used to construct the first-scattered distributed source for a discrete ordinates calculation with an $S_6$ triangular Chebychev-Legendre quadrature set, $P_5$ scattering and 39,011 tetrahedral cells. The water cross-sections were generated by CEPXS using the 37-group structure given in Table II.

**Table II. 37-group photon energy group structure.**

| Group | High E (MeV) | Low E (MeV) | Group | High E (MeV) | Low E (MeV) | Group | High E (MeV) | Low E (MeV) |
|---|---|---|---|---|---|---|---|---|
| 1 | 1.00 | 0.80 | 14 | 0.46 | 0.44 | 27 | 0.20 | 0.18 |
| 2 | 0.80 | 0.70 | 15 | 0.44 | 0.40 | 28 | 0.18 | 0.16 |
| 3 | 0.70 | 0.66 | 16 | 0.40 | 0.40 | 29 | 0.16 | 0.14 |
| 4 | 0.66 | 0.64 | 17 | 0.40 | 0.38 | 30 | 0.14 | 0.12 |
| 5 | 0.64 | 0.62 | 18 | 0.38 | 0.36 | 31 | 0.12 | 0.10 |
| 6 | 0.62 | 0.60 | 19 | 0.36 | 0.34 | 32 | 0.10 | 0.08 |
| 7 | 0.60 | 0.58 | 20 | 0.34 | 0.32 | 33 | 0.08 | 0.06 |
| 8 | 0.58 | 0.56 | 21 | 0.32 | 0.30 | 34 | 0.06 | 0.04 |
| 9 | 0.56 | 0.54 | 22 | 0.30 | 0.28 | 35 | 0.04 | 0.02 |
| 10 | 0.54 | 0.52 | 23 | 0.28 | 0.26 | 36 | 0.02 | 0.01 |
| 11 | 0.52 | 0.50 | 24 | 0.26 | 0.24 | 37 | 0.01 | 0.001 |
| 12 | 0.50 | 0.48 | 25 | 0.24 | 0.22 | | | |
| 13 | 0.48 | 0.46 | 26 | 0.22 | 0.20 | | | |

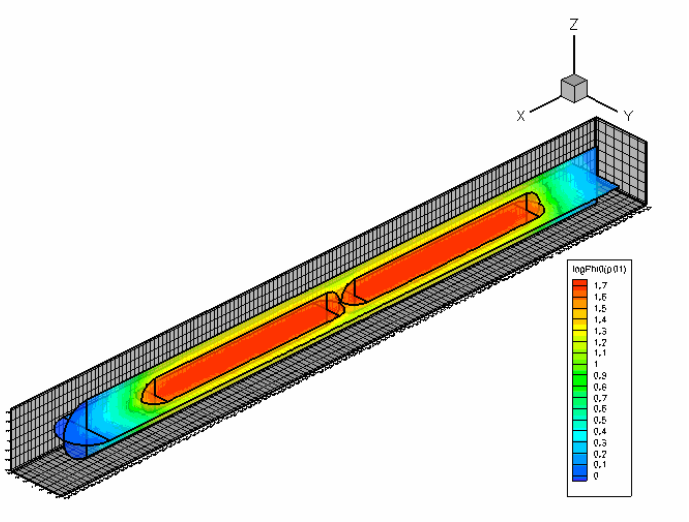


**Figure 6. $Log_{10}$ of photon scalar flux in the VS2000.**

### 3.2. MCNPX and Attila Phantom Results

Preliminary calculations in MCNPX showed that the inclusion of secondary electron transport unnecessarily consumed computing time (~40 times higher than photon-only transport: 392 minutes compared to 9 minutes) for 1e7 particle histories while not providing a substantially different solution for the scenario most likely to see buildup and subsequent approximate electronic equilibrium, namely bone near the source (see Fig. 7). Therefore, all results presented for MCNPX and Attila data are based on photon-only models.

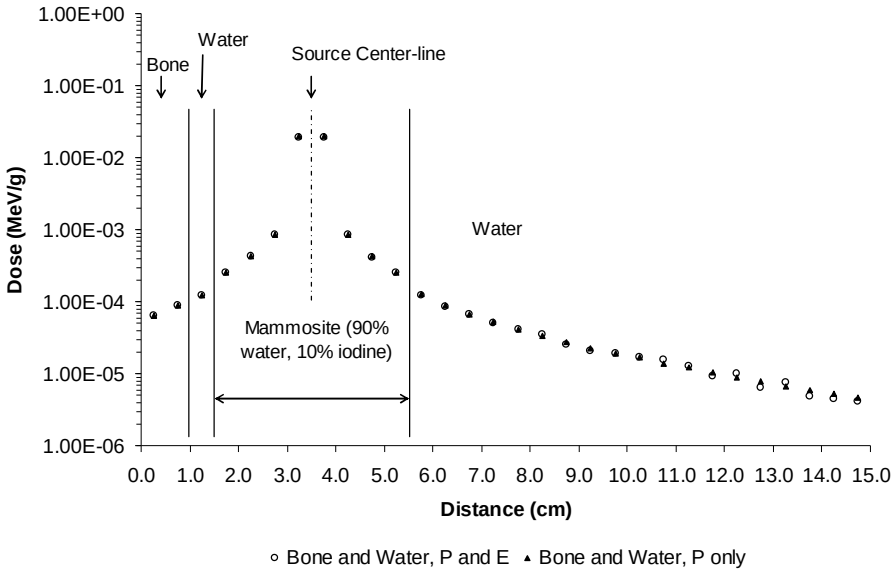


**Figure 7. Comparison between coupled photon-electron and photon-only transport in MCNPX**

Fig. 8 shows the graphical MCNPX mesh tally output (central plane of model) dose gradient of the all-water phantom model using a 0.5 cm voxel size. Note that the adjusted source strengths produce a uniform dose distribution about the balloon with the characteristic indention seen around the ends of a line source.

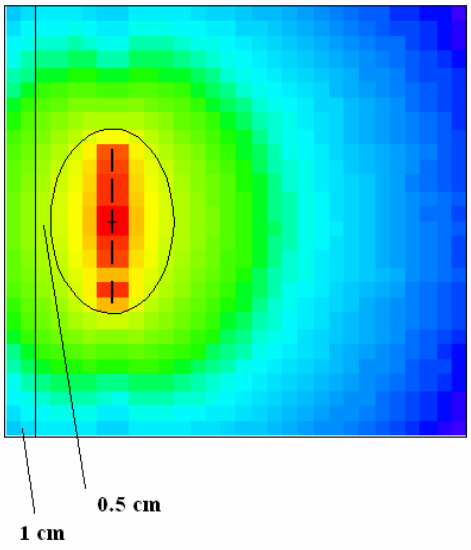


**Figure 8. MCNPX mesh tally water phantom results.**

Initial calculations consisted of dose (MeV/g) in each voxel normal to the central source center line in MCNPX and extending across bone, water, and air interfaces. Unlike Attila calculations, MCNPX mesh tallies are independent of the transport geometry and may cover more than one material. For this reason the code normalizes by cell volume, not mass, requiring results for each region of differing material to be divided by the density of that specific material. Relative errors for these calculations were all less than 0.02 and less than 0.01 in the regions of interest discussed here.

The source specification in Attila was adjusted from the previous simple model such that transport-corrected $P_2$ photon cross-section energy groups were reduced to 16, the number of tetrahedral cells increased to 68,000, and an $S_{50}$ square Chebychev-Lobatto quadrature set used. Simulation time for generating the anisotropic point source required tens of minutes, but is only performed once. Following source generation in Attila, three versions of the bone phantom model were simulated to investigate timing of the dose simulations. The first version incorporated a finer mesh in the bone and balloon, with a coarser mesh in the surrounding water ($S_8$, $P_4$ scattering, 68000 tetrahedral cells). A second version used a coarse mesh throughout the entire problem geometry ($S_8$, $P_4$ scattering, 2000 tetrahedral cells), and used an analytic ray trace to get uncollided dose at edit locations. The third version differed only from the second by a $S_4$ triangular Chebychev-Legendre quadrature set, $P_2$ scattering, and nearly 2000 tetrahedral cells. Fig. 9 shows the results for the bone phantom and the time savings achieved with negligible difference in results.

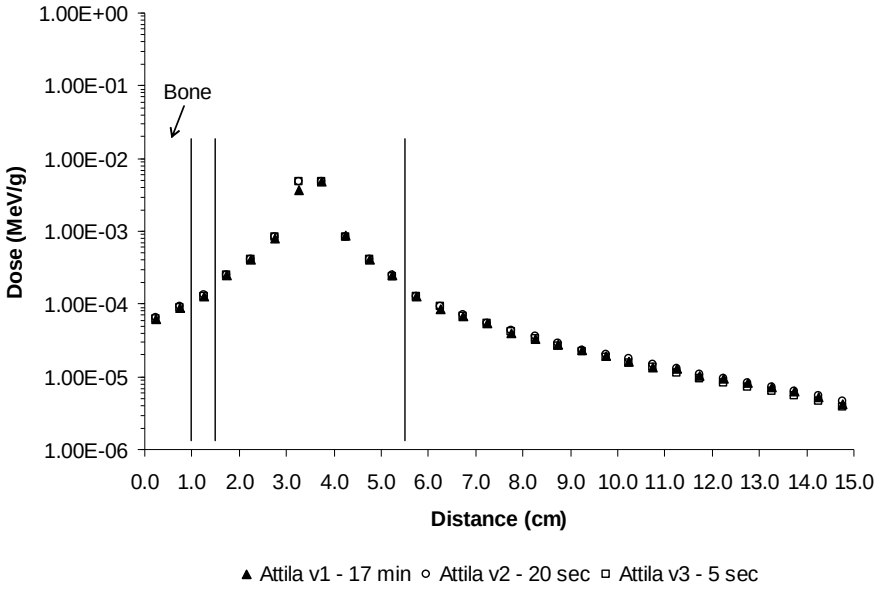


**Figure 9. Comparison of Attila simulation quality and timing.**

The data indicate agreement between MCNPX and Attila for the photon source energies of iridium-192. Differences in the materials given have little to no effect on dose deposition after crossing a boundary following the initial dose fall-off through the balloon contrast fluid. Percent differences in the bone region and water between the bone and balloon ranged from 1% to 2%. However, Attila gave values near the source between a factor of 4 and 6 lower than MCNPX (Fig. 10). This difference is related to the replacement of the volumetric VS2000 source with an equivalent self-shielded anisotropic point source.

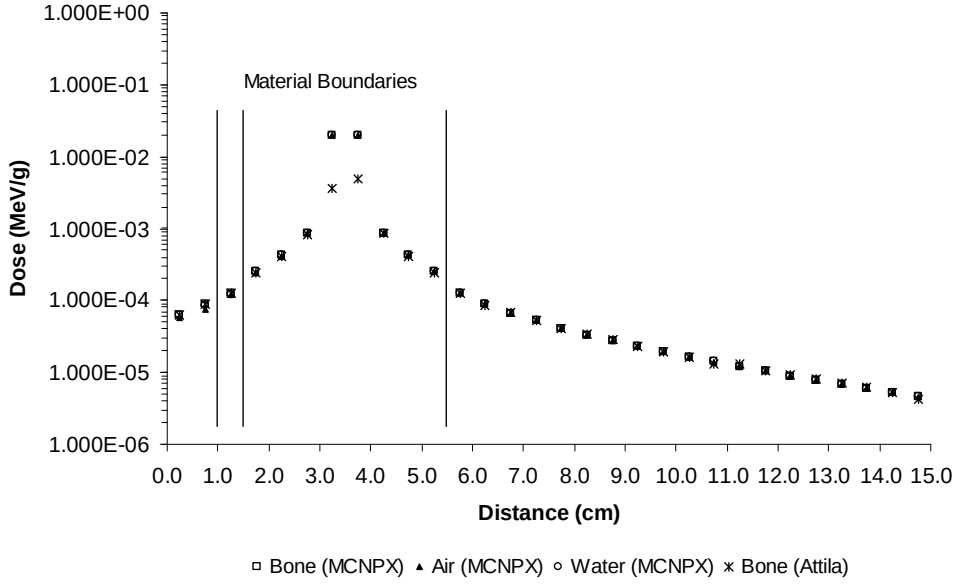


**Figure 10. MCNPX and Attila phantom model comparisons.**

While this process allows a computationally efficient simulation of the dose away from the source, the dose near the source is perturbed. [However, this dose can be obtained from the calculation used to compute the equivalent anisotropic point source.] Clinically, the dose in this region is not significant for the MammoSite applicator, but could be problematic for interstitial brachytherapy treatment modeling where sources are placed via catheter directly into the tissue volume.

### 3.3. Attila Patient-Specific Results

Current treatment planning software packages utilize empirical and/or semi-analytic radiation transport algorithms in patient specific geometries obtained by a variety of different imaging techniques, most commonly CT scans. Ultimately, more sophisticated transport treatments will be considered for treatment planning only if they can generate solutions on these geometries very quickly - on the order of minutes. There are several approaches to the transport of radiation through patient-specific geometries: 1) fine mesh transport through heterogeneous media (resolution equal to imaging resolution), or 2) coarse mesh transport utilizing homogenized interaction cross-sections. In many cases, coarse mesh transport provides reasonable accuracy for the calculation of particle fluxes, but it is very important that energy deposition (and dose) be calculated using the appropriate fine mesh material properties (kerma interaction cross-sections and densities). In this work, the commercial package Scan2MCNP was investigated to generate geometries for MCNPX directly from DICOM format CT images. The initial intent was to use a fine mesh to resolve the spatial heterogeneities given in the CT scans, but the sheer number of cells (approximately 46,000 for twenty-three 3 mm slices) and the increased number of photon histories required to obtain statistically significant dose calculations made this approach intractable. Fine-mesh deterministic transport calculations of these systems will be more computationally efficient, but it is likely that simulation times would still be too long. An example coarse mesh deterministic transport calculation of the MammoSite implanted in a patient-specific geometry has been performed with a prototypical version of Attila. Fig. 11 shows a single 3 mm slice of the 3-dimensional CT data of the anatomical geometry used in the Attila simulation, and dose contours are presented in Fig. 12.

**Figure 11. Patient CT image of implanted MammoSite device.**

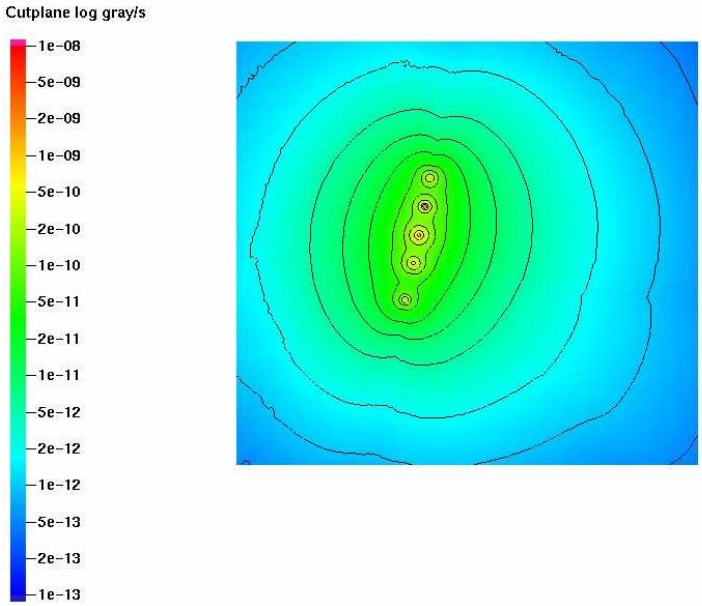


**Figure 12. Attila-generated (coarse mesh) isodose contour lines in patient specific geometry (provided by Transpire, Inc.).**

This result is included here as a demonstration of capability. The detailed problem specification will not be presented, but this calculation, from the reading of CT images to the three dimensional computation of dose, was completed in 1.5 minutes. A similar calculation has not been completed with MCNPX; plans to finish the patient specific comparison will be left for future work.

## 4. CONCLUSIONS

Verified by MCNPX, Attila is a viable option for potential brachytherapy treatment planning of the MammoSite device using deterministic radiation transport methods. While Monte Carlo methods were used here to demonstrate equivalent physics modeling, the MCNPX limitation of volume-normalized meshes prevents its use for large-scale treatment planning where material heterogeneity is prevalent. Additionally, longer computing times are anticipated with Monte Carlo transport through increasingly finer meshes with a low error requirement, as compared to Attila, where results are calculated globally throughout the spatial mesh. Although not quite as computationally efficient as current algorithm-based treatment planning, Attila does accurately account for differences in materials. This aspect could allow for greater freedom in medical device design, which is currently limited to tissue/water equivalent materials because of treatment planning software limitations.

## ACKNOWLEDGEMENTS

The authors would like to thank Dr. Tony He of Oregon Health & Science University for the use of patient CT images and Dr. Todd Wareing and Ian Davis of Transpire, Inc. for their assistance in the Attila calculations.

## REFERENCES

[1] R. Nath, et al. "Dosimetry of interstitial brachytherapy sources: Recommendations of the AAPM Radiation Therapy Committee Task Group No. 43," *Medical Physics*, **22(2)**, pp.209-233 (1995).
[2] M. J. Rivard, et al. "Update of AAPM Task Group No. 43 Report: A revised AAPM protocol for brachytherapy dose calculations," *Medical Physics*, **31(3)**, pp.633-674 (2004).
[3] I. J. Chetty, "Monte Carlo Treatment Planning: The Influence of 'Variance Reduction' Techniques (ECUT, PCUT, ESTEP) on the Accuracy and Speed of Dose Calculations," *Medical Physics*, **32(6)**, p.2018 (2005).
[4] K.A. Gifford, et al. "Comparison of a finite-element multigroup discrete-ordinates code with Monte Carlo for radiotherapy calculations," *Physics in Medicine and Biology*, **51(9)**, pp.2253-2265 (2006).
[5] Nuclear Regulatory Commission Registry of Radioactive Sealed Sources and Devices, Registry Number CA1080S102S (2001).
[6] G. P. Glasgow and L. T. Dillman, "Specific γ-ray constant and exposure rate constant of $^{192}$Ir," *Medical Physics*, **6(1)**, pp.49-52 (1979).
[7] A. Angelopoulos, et al. "Monte Carlo dosimetry of a new $^{192}$Ir high dose rate brachytherapy source," *Medical Physics*, **27(11)**, pp.2521-2527 (2000).
[8] G. K. Edmundson, et al. "Dosimetric characteristics of the MammoSite RTS, a new breast brachytherapy applicator," *International Journal of Radiation Oncology, Biology, Physics*, **52(4)**, pp.1132-1139 (2002).